COBEM 2023 27TH INTERNATIONAL CONGRESS OF MECHANICAL ENGENEERING

ABCM Brazilian Society of Mechanical Sciences and Engineering
27th ABCM International Congress of Mechanical Engineering
December 04-08, 2023, Florianópolis-SC, Brazil

COB-2023- 0673
ANALYSIS OF OPTIMAL FIN SPACING FOR ENHANCED HEAT TRANSFER IN HORIZONTAL TUBES

Sandi Itamar Schafer de Souza
Universidade Federal do Rio Grande do Norte, Centro de Tecnologia, Departamento de Engenharia Mecânica, Campus Universitário Lagoa Nova, Av. Senador Salgado Filho, n° 3000, CEP 59078-900, Natal, Rio Grande do Norte, Brasil
sandi.souza@ufrn.br
Thiago Cardoso de Souza
Universidade Federal de Santa Catarina, Centro Tecnológico, Departamento de Engenharia Mecânica, Caixa Postal 476, Campus Universitário, Trindade, CEP 88040-900, Florianópolis, SC, Brasil
t.cardoso@ufsc.br

Abstract. *This study focuses on the coupling between free convection heat transfer phenomena and turbulent internal flow in a horizontal tube with annular fins. By considering a well-known configuration, this investigation aims to determine the optimal fin spacing for maximizing heat transfer. Seven configurations with fin spacing of 2.5 mm, 3.5 mm, 5 mm, 7.5 mm, 10 mm, 15 mm and 20 mm were analyzed, taking into account axial heat conduction and finned tube performance. For all cases investigated, a geometric model with three domains was used, consisting of two fluid domains (heated water as the internal forced flow through the main tube and air in the outside region) and a solid domain composed of a finned steel tube. The governing differential equations were solved using a commercial CFD solver. Through the variation of the spacing between the applied fins, the existence of an optimal fin configuration associated with maximum heat transfer, dependent on the optimum distance between the fins, was verified. The results show that thermal changes vary according to the fin position and spacing between the fins. A more realistic modeling of the temperature distribution in the fluid and the appropriate consideration of heat conduction effects confirmed the existence of conditions for maximum heat transfer depending on the distance between the applied fins. The study provides valuable insights to optimize the design of finned tubes for enhanced heat transfer performance in practical applications*.

Keywords: *Finned tube, Convective Heat Transfer, Optimal Fin Spacing, Numerical simulation*

1. INTRODUCTION

Fins are extended surfaces used in numerous industrial applications to intensify heat transfer from a solid to a fluid. These devices are used in heating and cooling systems, heat exchangers, and controlled ventilation systems, among others, enabling, for instance, a reduction in the size of these systems. The heat transfer in finned tubes has been studied both experimentally and through the solution of the governing equations using analytical and numerical methods. However, the analytical solutions have limited applicability since these approaches often employ boundary conditions that may deviate from physical reality, such as for instance the assumption of a constant prescribed temperature on the wall. Incropera et al. (2007) and Bejan (2013) state that in free convection, the fluid moves due to buoyancy forces, whereas in forced convection, motion is imposed by some external source. According to Bejan (2013), temperature variation is the driving force of free convection with the buoyant force being generated due to the presence of a density gradient in the fluid. For convective heat transfer problems involving complex geometries, numerical simulations prove to be a valuable tool, enabling a better understanding of the behavior of the variables that govern the phenomenon.

For practical purposes, the design of the finned tube incorporates some significant assumptions. For example, a constant convective coefficient is often assumed over the fin surface, despite the knowledge that the fluid flow and the presence of the base surface create a complex flow around the solid. Kayansayan and Karabacak (1992) show that the Nusselt number of fin-tubes as a function of Rayleigh is generally lower when compared to a smooth tube without fins. Furthermore, no single correlation for the Nusselt number incorporates all geometric possibilities. It is known that the convective coefficient depends on the geometry, thus it may be necessary to adopt other simplifying assumptions, which can lead the solution far from physical reality.

The phenomenon of heat transfer in a finned tube configuration is halfway between heat transfer in a non-finned tube and heat transfer between parallel plates. Notable early research in this area includes the work of Elembaas (1942), who studied free convection in heated parallel vertical plates, demonstrating that the Nusselt number depends not only on the Grashoft and Prandtl numbers, but also on the ratio between the fin spacing (S) and the fin height (H). Bar-Cohen and Rohsenow (1984) investigated the optimal spacing in heated vertical plates subjected to free convection. They used an analytical approach to identify the limit situation, where the thermal effects of one plate do not interfere with those of another. Yaghoubi and Mahdavi (2013) sought convective coefficients and correlations for the Nusselt number for finned

tubes, using numerical and experimental techniques to study free convection in tubes with aluminum fins. Souza et al. (2019) presented results for heat transfer in finned tubes, using numerical simulation and considering a prescribed temperature on the tube wall to identify an optimal point for heat transfer.

Thus, this study aims to complement the referred investigations while focusing on the numerical analysis of the influence of fin spacing, without employing the simplified assumption of a constant prescribed temperature on the wall. For this purpose, a geometric model was developed with three distinct domains: water, steel, and air. To solve the transport equations numerically, we used a commercial CFD solver (ANSYS-CFX-2023).

2. PHYSICAL MODEL, COMPUTATIONAL MESH AND BOUNDARY CONDITIONS

The simulations developed in this work are divided into two stages. Initially, simulations for water flow in a smooth tube were carried out. An adiabatic wall condition in the tube is imposed, along with a set of boundary conditions at the inlet, with a prescribed temperature of 100 °C and an inlet normal velocity of 0.5 m/s. This ensures that the Reynolds number of the main flow is approximately 4.2×10^4. A constant static pressure boundary condition at the outlet is imposed. The length (L) of the tube is set to 2.5 m, ensuring that the condition of fully developed flow is achieved at the tube outlet. In the first stage, temperature, velocity, turbulent kinetic energy, and turbulent viscosity fields are extracted at the tube exit to provide an inlet condition for the simulations of the finned tube configuration. In the smooth tube flow simulation, turbulence is modeled with the SST turbulence model in combination with a turbulent intensity of 5% as the turbulent inlet boundary condition.

In the second stage, the simulation of a finned tube configuration consisting of a set of 35 fins is performed. Due to limited computational capacity, the set is divided into five parts. Each domain used has six fins with a thickness of t and two half-fins, $t/2$, at the ends. Figure 1 shows the physical model used in this study, consisting of three subdomains: two fluid domains and one solid domain. Flow symmetry is considered along the main tube centerline. Table 1 shows the values of the main dimensions of the model used. Figure 2 illustrates the hexahedral mesh used in these simulations, consisting of 2.21×10^6 nodes.

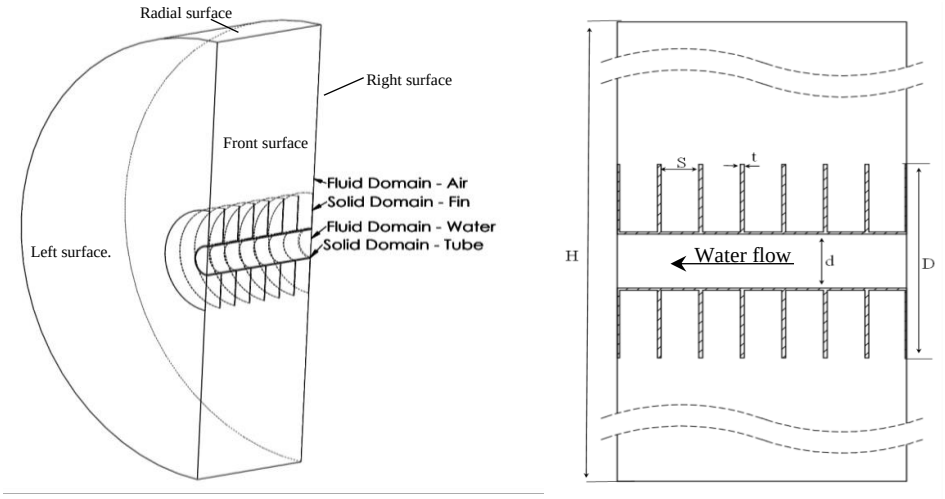

Figure 1: Physical domain used.

Table 1 – Spatial dimensions of the model used.

Dimension	**Value**
S (mm)	2.5, 3.5, 5, 7.5, 10, 15, 20
d (mm)	25.4
D	3.5 d
t (mm)	0.5
H	10 D

The simulations were run under a steady-state condition, with fully developed turbulent flow in the main tube. In the external domain, the fluid is air, where laminar free convection is established. For the solid domain, which consists of the finned tube, the material is steel. In the first part of the domain, e.g., consisting of 6 simulated fins, as shown in Figure 1, the outlet results of the previously simulated tube were used as the inlet boundary condition for the water flowing in the main tube. This characterizes a fully developed flow with a fluid temperature of 100 °C. The outlet surface of the water domain maintained a constant pressure equal to atmospheric pressure. The radial surface of the air domain is considered

an open surface at a temperature of 25 °C. On the external surfaces of the model, both right and left, symmetry boundary conditions are imposed. Symmetry is also imposed on the frontal surface for all regions: fin, air, and water. The problem contains two fluid-solid interfaces, one associated with the water flow in the main tube and the associated applied fins and the other domain consisting of air and the finned tube.

As mentioned earlier, the entire domain is divided into five parts. For the other four domains of six simulated fins, the results from the outlet of the previously simulated domain were used as the inlet boundary condition for the water flow, while keeping the remaining boundary conditions the same as in the previous domains.

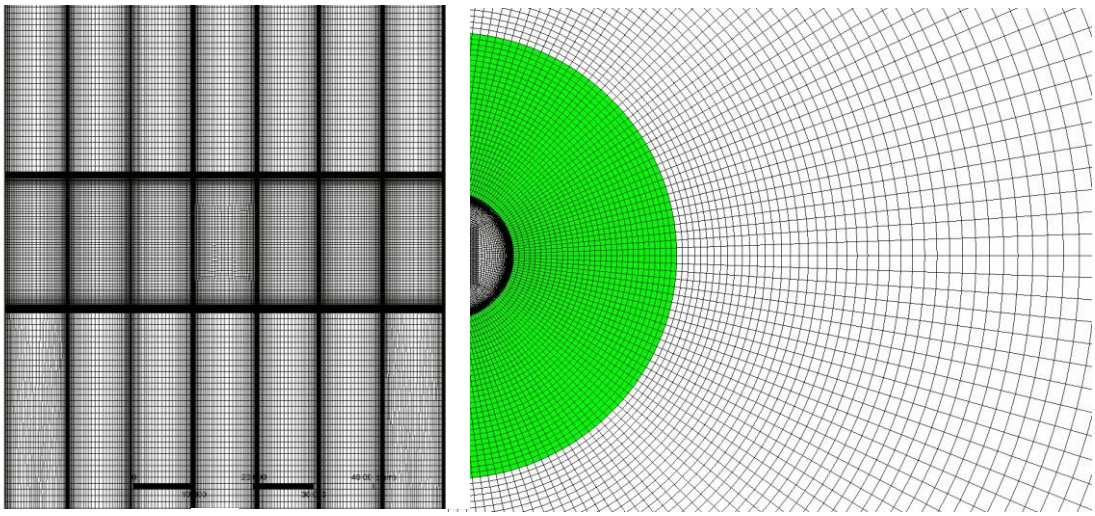

a b

Figure 2: a) Front view of the mesh (Fluid domain, inner tube, and fins) b) Mesh in all domains.

3. GOVERNING EQUATIONS

To conduct a preliminary assessment of the flow regime in the domain where the working fluid is air and free convection occurs, the Rayleigh number, Eq. (1), was computed, such that for this case *Ra* equals to 2.5×10^5, which indicates a laminar convective flow regime.

$$Ra = \frac{g\beta\left(T_\infty - T_w\right)D_f^3}{\nu\alpha} \tag{1}$$

Since air heating results in a decrease in the specific mass value of the fluid and a consequent upward movement due to the buoyancy forces generated, the flow in the emerging plume will be laminar if the Grashoff number value, as per Eq. (2), is less than 6.4×10^7, Bill and Gebhart (1974).

$$Gr_y = \frac{g\beta\left(T_\infty - T_w\right)\left(\frac{H}{2}\right)^3}{\nu^2}, \tag{2}$$

where g represents the acceleration due to gravity. The variables D_f, β, υ, H, and α denote the fin's diameter, volumetric thermal expansion coefficient, kinematic viscosity, vertical distance, and the thermal diffusivity of air at mean temperature, respectively. The vertical distance, H, from the fin to the upper region of the domain is selected in order to ensure that the flow remained in the laminar regime.

Closely following Wilcox (1993), Kundu (1990), and Bejan (2013), the free convective laminar flow external to the finned tube, is solved using the continuity equation in combination to the Navier-Stokes equations (Eq. (3) and Eq. (4)), based on an incompressible fluid assumption. Heat transfer processes are modelled by the corresponding energy conservation equation, Eq. (5), with Eq. (5) corresponding to the fluid domain and Eq. (6), the conduction equation, for the solid domain,

$$\frac{\partial}{\partial x_j}\left(\rho u_j\right) = 0\,, \tag{3}$$

$$\frac{\partial}{\partial x_j}\left(\rho u_i u_j\right) = -\frac{\partial p}{\partial x_i} + \frac{\partial}{\partial x_j}\left[\mu\left(\frac{\partial u_i}{\partial x_j} + \frac{\partial u_j}{\partial x_i}\right)\right] + S_M\,, \tag{4}$$

$$\frac{\partial}{\partial x_j}\left(\rho u_j T\right) = \frac{\partial}{\partial x_j}\left(\frac{k_f}{c_p}\frac{\partial T}{\partial x_j}\right), \tag{5}$$

$$\frac{\partial}{\partial x_j}\left(k_s \frac{\partial T}{\partial x_j}\right) = 0\,, \tag{6}$$

where u_i is the instantaneous velocity in tensor notation, x_i is the position in index notation. The variables p, T, Cp, k, and ρ represent the pressure, temperature, specific heat at constant pressure, thermal conductivity, and specific mass, respectively. S_M represents the body forces (Buoyancy Force), for instance, when including the buoyancy force, the source term (Eq. (7)) is added to the momentum equations (Eq. (4)) based on the difference between the fluid's specific mass (ρ) and a reference density (ρ_{ref}). The specific mass difference was evaluated using the Full Buoyancy model.

$$S_M = g\left(\rho - \rho_{ref}\right) \tag{7}$$

To model the turbulent flow of water inside the tube, a RANS formulated approach is used considering the following equations:

$$\frac{\partial}{\partial x_j}\left(\rho U_j\right) = 0\,, \tag{8}$$

$$\frac{\partial}{\partial x_j}\left(\rho U_i U_j\right) = -\frac{\partial P}{\partial x_i} + \frac{\partial}{\partial x_j}\left[\mu\left(\frac{\partial U_i}{\partial x_j} + \frac{\partial U_j}{\partial x_i}\right) - \overline{\rho u_j' u_i'}\right], \tag{9}$$

$$U_j \frac{\partial}{\partial x_j}\left(\overline{T}\right) = \frac{\partial}{\partial x_j}\left(\alpha \frac{\partial \overline{T}}{\partial x_j} - \overline{u_j T'}\right) \tag{10}$$

Here, U represents the mean velocity in tensor notation, P represents the mean static pressure, and $\overline{T}$ is the mean temperature, while T' and u' represent the temperature and velocity fluctuations due to turbulence, respectively. To model the turbulent flow of hot water inside the tube, the SST turbulence model, as described by Menter (2003) and Menter (1994), is considered. This model uses the definition of turbulent viscosity defined by Eq. (11),

$$\nu_t = \frac{a_1 k}{\max\left(a_1\omega, SF_2\right)}\,, \tag{11}$$

where S is the invariant measure of the strain rate, and a_1 is a constant. The model employs the following transport equations for turbulent kinetic energy (k) (Eq. (12)) and the rate of dissipation (ω) (Eq. (13)),

$$\frac{\partial}{\partial x_i}\left(\rho U_i k\right) = \tilde{P}_k - \beta^* \rho k\omega + \frac{\partial}{\partial x_i}\left[\left(\mu + \sigma_k \mu_t\right)\frac{\partial u_i}{\partial x_i}\right], \tag{12}$$

$$\frac{\partial}{\partial x_i}\left(\rho U_i \omega\right) = \alpha\rho S^2 - \beta\rho\omega^2 + \frac{\partial}{\partial x_i}\left[\left(\mu + \sigma_\omega \mu_t\right)\frac{\partial \omega}{\partial x_i}\right] + 2(1-F_1)\rho\sigma_{w2}\frac{1}{\omega}\frac{\partial k}{\partial x_i}\frac{\partial \omega}{\partial x_i}\,, \tag{13}$$

where the first and second blending factors, F_1 and F_2 are defined by de Eq. (14) and Eq. (16), respectively.

$$F_1 = \tanh\left\{\left\{\text{`min}\left[\max\left(\frac{\sqrt{k}}{\beta^*\omega y}, \frac{500\nu}{y^2\omega}\right), \frac{4\rho\sigma_{\omega 2}k}{CD_{k\omega}y^2}\right]\right\}^4\right\}, \tag{14}$$

$$CD_{k\omega} = \max\left(2\rho\sigma_{\omega 2}\frac{1}{\omega}\frac{\partial k}{\partial x_i}\frac{\partial \omega}{\partial x_i}, 10^{-10}\right), \tag{15}$$

$$F_2 = \tanh\left[\left[\max\left(\frac{2\sqrt{k}}{\beta^*\omega y}, \frac{500\nu}{y^2\omega}\right)\right]^2\right], \tag{16}$$

$$P_k = \mu_t\frac{\partial U_i}{\partial x_i}\left(\frac{\partial U_i}{\partial x_j} + \frac{\partial U_j}{\partial x_i}\right) \quad \rightarrow \quad \tilde{P}_k = \min\left(P_k, 10\beta^*\rho k\omega\right) \tag{17}$$

In this model, the coordinate y represents the distance from the non-slip boundary, and the other constants are all derived from the k–ε and k–ω models, with some adjustments, as described by Menter et al. (2003): a_1=0.31, β*= 0.09, α_1 =5/9, β_1= 0.075, σ_k= 0.85, $\sigma_{\omega 1}$=0.5, α_2 =0.44, β_2 = 0.0828, σ_{k2} = 1, and $\sigma_{\omega 2}$ = 0.856. The full set of governing equations are solved using a commercial CFD solver, namely ANSYS-CFX-2023, with a convergence criterion adopted in terms of a RMS value of 1.0x10^{-6} for all velocities, temperatures, energies, and pressures.

4. MESH INDEPENDENCE

Mesh independence test was performed using the physical model shown in Figure 1 with the dimensions shown in Table 1 and for the case with a spacing (S) of 5 mm. Eight meshes were considered, and the results are presented in Figure 3. It can be observed that mesh independence already occurs when the number of nodes exceeds 8x10^6, when a heat transfer rate of 11.5 W is considered as the reference value to determine the relative difference between the solutions. Given the available computational resources, the mesh with 2.21x10^6 nodes is considered as the reference mesh resolution of this paper, this resolution provided results for the heat transfer rate with a relative difference on the order of 1%.

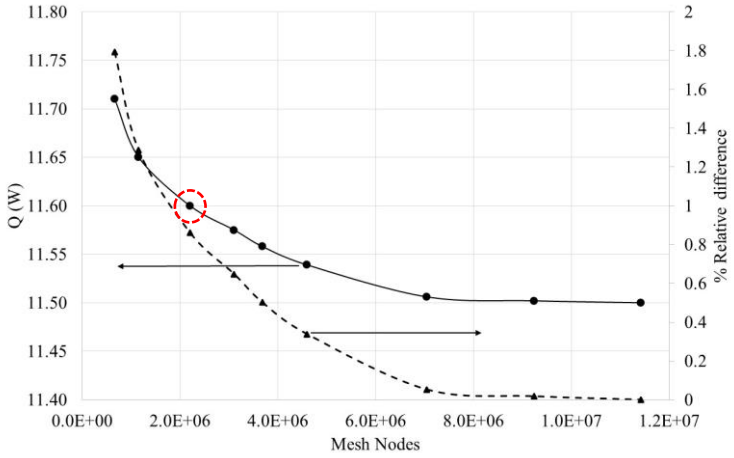

Figure 3: Mesh independence study.

5. RESULTS

Figure 4 shows the behavior of temperature along three lines positioned inside the steel tube for the case in which the fin spacing (S) is 5 mm. Considering the angle θ to be 0 at the top, the lines were placed at three positions with a radius of 13.2 mm and angular positions of θ equal to 0º, 90º, and 180º along the entire length of the tube. Initially, it can be noted that temperatures vary with the angular position, with the lowest temperatures occurring in the bottom region (θ=180º) and the highest temperatures in the top region (θ=0º). Along all lines, there are fluctuations in temperature, with maximum and minimum values. In the tube, at points where the fins are positioned and heat is transferred from the tube to the fin, a minimum appear, indicating lower temperatures. Conversely, in the areas between the fins, where heat is

transferred from the tube to the air, temperatures reach their maximum values in the center of this space, indicating that axial conduction is present in the tube, particularly in the region between the fins.

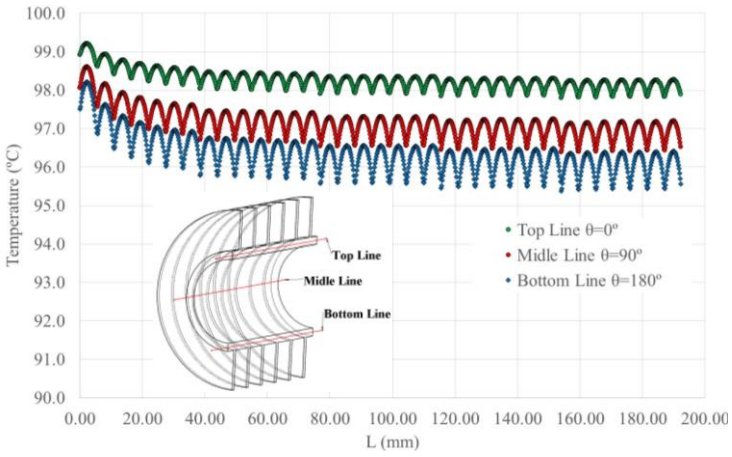

Figure 4: Temperature in three lines inside the tube domain.

Figure 5 presents the behavior of the average temperature recorded at the air-tube and air-fin interfaces as a function of spacing. It can be observed that the average temperature initially decreases as the separation increases. For the air-fin interface, when the spacing *S* equals 10 mm, the average temperature shows a constant behavior. However, for the air-tube interface, a minimum point occurs at *S* equal to 7.5 mm, after which the average temperature begins to increase again. This effect can also be observed in Figure 6, where the temperature field at the three interfaces, air-tube, air-fins, and fin-tube is presented for six studied *S* spacings: 2.5 mm, 3.5 mm, 5 mm, 7.5 mm, 10 mm, and 15 mm, for the fifth (last group) group of six fins that comprise the simulated domain. Based on the color gradient, it can be seen that the temperature difference at the air-fin interface is around 10 ºC for *S* spacing of 2.5 mm, around 15 ºC for an *S* spacing of 3.5 mm, and around 25 ºC for *S* spacings of 5 mm, 7.5 mm, and 10 mm.

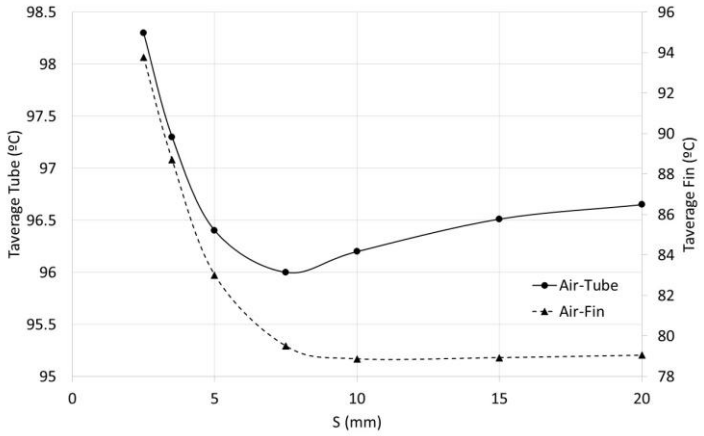

Figure 5: Average temperature in fin and tube surfaces.

The larger the spacing, the lower the temperatures at this interface, which is due to the increased intensity of heat transfer. On the external tube wall, the highest temperatures occur at the smallest *S* spacings. The lowest temperatures are recorded at the fin-tube interface, corroborating the data presented in Figure. 4. This is due to heat conduction between the fin and the tube, which is more intense than the convection between the tube and the air. The cooling of the tube wall, as a result of heat transfer, reaches its maximum point when *S* equals 7.5 mm. However, for spacings larger than 7.5 mm, the intensity of heat transfer decreases, resulting in a slight increase in the average temperature in this region.

The contours of temperature, velocity magnitude, and buoyant force in three vertical planes are shown in Figure 7 for six investigated cases. The heating of the air by the tube and the fin assembly alters the specific mass of the fluid. In the presence of the gravitational field, this effect promotes the existence of buoyant forces and the consequent movement of the air, responsible for the occurrence of free convection. In Figure 7, when S is less than 5 mm, low-intensity temperature gradients can be identified in the region between the fins, especially in the lower region. Here, the ambient temperature

air comes into contact with the heated fins, and in these spaces, the lowest velocities occur. The boundary layer that forms extends to the entire length of the channel formed by the fins. In the flow between the fins, buoyant forces compete with viscous forces, which are imposed by the walls. In smaller gaps, maximum buoyancy occurs in almost the entire region between the fins. In these positions, the values of the buoyant force are higher and are counterbalanced by viscous effects. This is shown in Figure 8, which presents the relationship between the buoyant force in the air (in the volume between the fins) and the shear forces acting on the walls, as defined by Eq. (18).

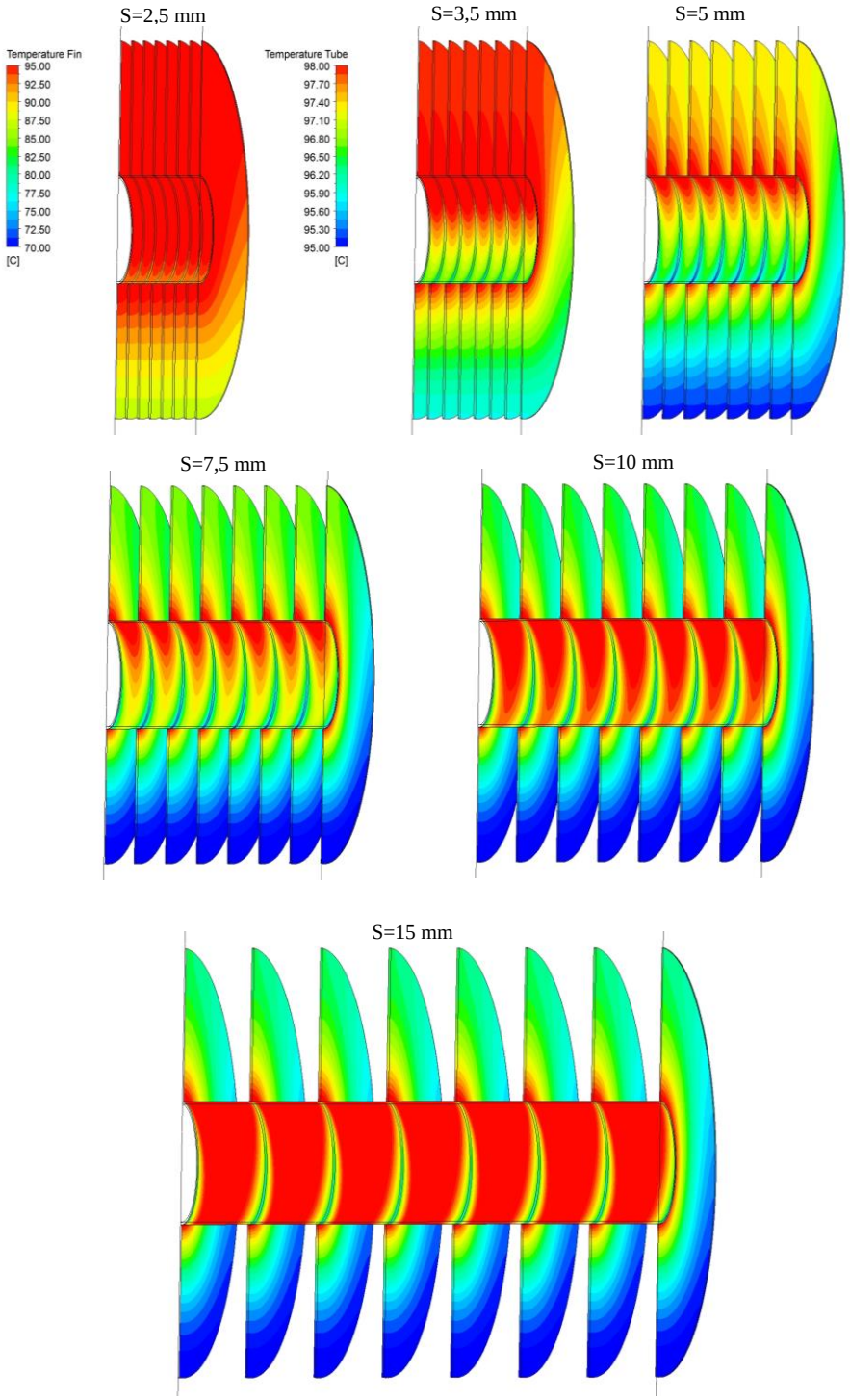

Figure 6: Temperature fields on the external wall of the tube and on the fin walls.

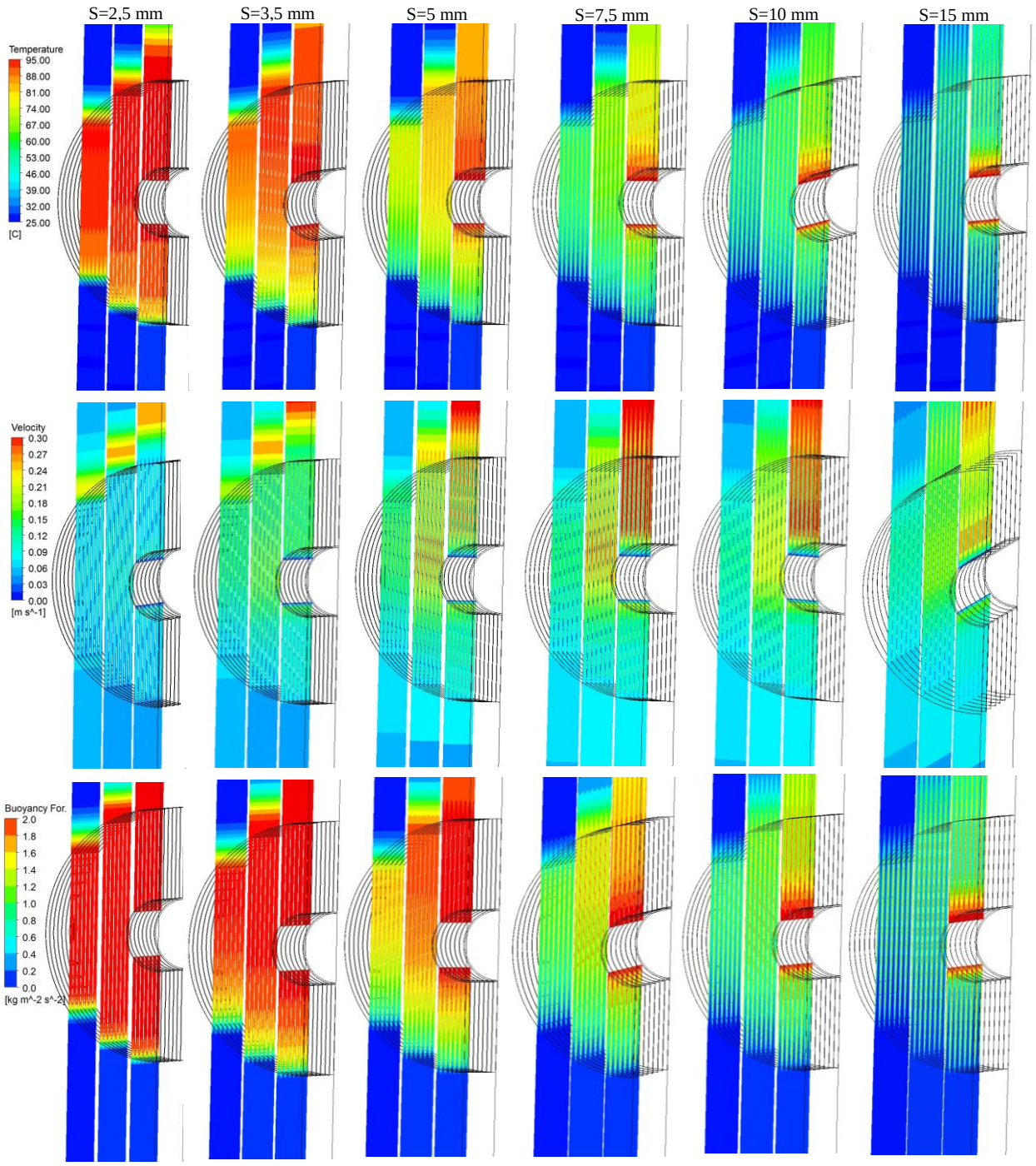

Figure 7: Temperature fields, velocities, and buoyant forces in the air, for three vertical planes.

$$\frac{F_{Buoyancy}}{\mathrm{F}_{Shear}} = \frac{\int \left[g\left(\rho - \rho_{ref}\right) \right] d\forall_{Air} \Big/ \forall_{Air}}{\int \tau_w dA_{tube} + \int \tau_w dA_{fin} \Big/ \forall_{Air}}, \tag{18}$$

here, $\forall_{air}$ is the volume occupied by the air between the fins, $F_{Buoyancy}$ and F_{Shear} represent the buoyant and the shear forces per unit of volume, τ_w is the wall shear stress, and A_{tub} and A_{fin} are the surfaces of the tube and the fins, respectively.

The mass flow between the fins is influenced by the balance of these forces, as explained by Incropera (2007). The viscous effect is more pronounced for smaller gaps, leading to a reduction in mass flow. As the gap, S, increases, the viscous effect diminishes, resulting in increased mass flow. For values of S greater than 3.5 mm, a decrease in the temperature field and an increase in the velocity field can be observed in Figure 7. At an S spacing greater than 10 mm, in the vertical plane furthest from the tube, the air temperature in the central region of the channel hovers around 25 °C.

This suggests that the thermal boundary layers does not intersect, which diminishes the buoyant effect and leads to reduced air velocity.

Figure 8 shows that for spacings of *S* less than 10 mm, mass flow in the gap augments with the increase in the $F_{Buoyancy}/F_{Shear}$ ratio, peaking at an S spacing of 10 mm. For spacings of S larger than 10 mm, the mass flow declines, even with an increase in the $F_{Buoyancy}/F_{Shear}$ ratio, since the boundary layers do not intersect. When *S* is less than 5 mm, the buoyancy effect is intensified throughout the spacing between the fins. However, the values of the $F_{Buoyancy}/F_{Shear}$ ratio are approximately one, indicating that heat transfer by conduction is dominant in these regions. For spacings greater than 3.5 mm, when the $F_{Buoyancy}/F_{Shear}$ ratio exceeds one, convective heat transfer becomes dominant. This observation aligns with the findings in both Figure 7 and Figure 8.

For an *S* spacing of 15 mm, the temperature and velocity fields are less pronounced than in cases where *S* spacings are 5 mm, 7.5 mm, or 10 mm, in which the thermal boundary layers intersect. The change in the specific mass of the air will be less substantial at a spacing of 15 mm, resulting in slower velocities at the center of the channel formed by the fins, compared to smaller spacings. The non-intersection of the boundary layers, as can be observed from an *S* spacing of 10 mm, persists for larger spacings. Consequently, the heat transfer rate of the fins remains stable, as shown in Figure 9. This pattern explains why the average temperature in the tube reaches its lowest value at a spacing of 7.5 mm and then rises with increased spacing, as seen in Figure 5. It also sheds light on the behavior of the average temperature on the fin, which remains virtually constant from a spacing of 10 mm onwards, as illustrated in Figure 5.

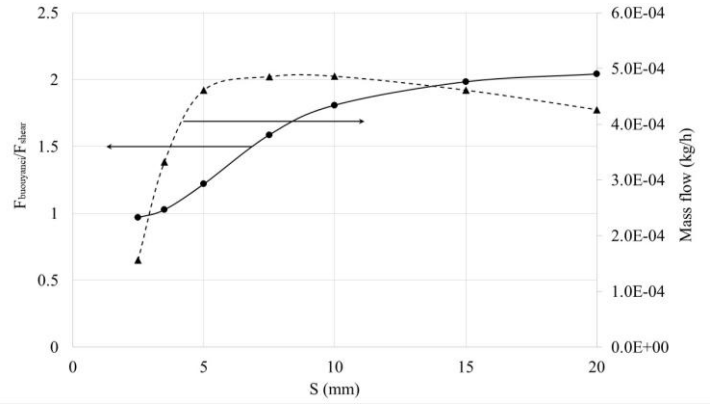

Figure 8: Relationship between buoyant forces and Shear forces, and the mass flow, in the region between the fins.

Figure 9 shows the heat transfer rates for the fifth set of fins, delineating the portions of the rates transferred by the air-tube interface, the air-fin interface, and the total contribution. It is evident that the portion from the air-fin interface assumes an almost constant behavior from a spacing of 10 mm, analogous to the observed behavior for the average temperature of the fins, as shown in Figure 5. This consistency can be attributed to the flow behavior around the fins. However, the rate transferred at the air-tube interface escalates with increased spacing. Such an observation might initially seem contradictory when considering the behavior of the average temperature at this interface. Despite the decline in the magnitude of the velocity field surrounding the tube, as illustrated in Figure 6, the expansion in spacing contributes to a larger exchange surface, thereby enhancing the heat transfer rate to the air.

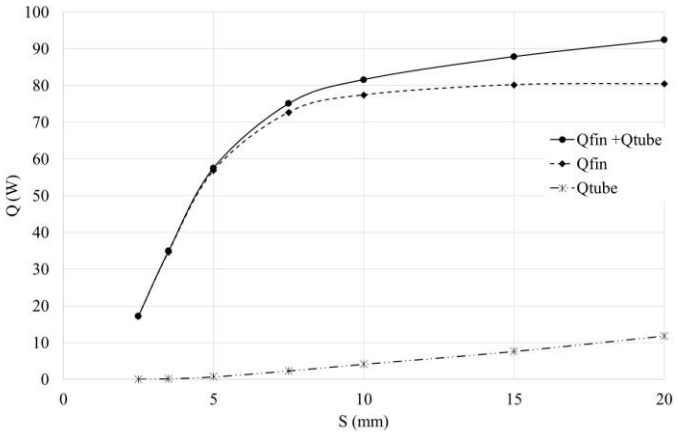

Figure 9: Heat transfer rates for the set of 35 fins.

When investigating the optimal spacing, the heat rate of the fin-tube set (35 fins plus tube) is divided by the length of the set. This is shown in Figure 10, which shows that there is a maximum point for a spacing of 5 mm.

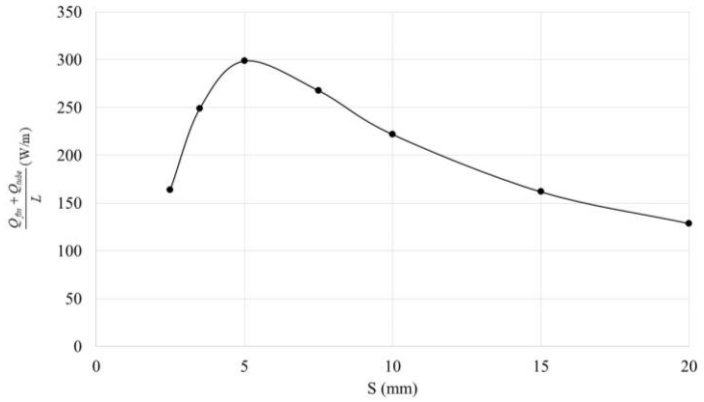

Figure 10: Heat transfer rates per unit length for the set of 35 fins.

6. CONCLUSIONS

The results indicate that the spacing of the fins affects the balance between buoyant and viscous forces, causing low mass flow rates to traverse the channel formed by the fins at smaller spacings, thereby hindering heat exchange via convection. The highest velocities within the channels formed by the fins are observed for spacings between 3.5 mm and 10 mm, corresponding to the highest heat transfer rates per linear length. Starting from a spacing of 10 mm, the rate of heat transfer by the fins becomes constant, and beyond this point, the flow between the fins changes minimally, similar to the situation observed with vertical flat plates where boundary layers do not intersect. Beyond this spacing, the increase in the heat transfer rate is attributable mostly to the increase in the tube's exchange section. Clearly, there is an optimal point, which occurs when the spacing is 5 mm. The results demonstrate that the assumption of a constant temperature on the fins or on the tube wall produces outcomes distant from physical reality, as temperature differences of the order of 35 ºC occur at the air-fin interfaces, and differences of approximately 3 ºC are present at the air-tube and fin-tube interfaces. The temperatures on the tube wall and the fin fluctuate based on the angular position, radial position, and axial position.

7. REFERENCES

Bar-Cohen, A., Rohsenow W. M., 1894. “Thermally optimum spacing of vertical, natural convection cooled, parallel plates”. Transactions of the ASME, Vol. 106, pp. 116-123.

Bejan, A. 2013. *Convective heat transfer*. John Wiley & Sons, New York.

Bill Jr, R. G., Gebhart, B., 1974. “The Transition of plane plumes”. Int. J. Heat Mass Transfer, Vol. 18, pp. 513-526.

Elenbaas, W., 1942. “Heat dissipation of parallel plates by free convection”. Phisica 9, Vol. 1, pp.1-29.

Incropera, F.P., D.P. DeWitt, T.L. Bergman, and Lavine, A. S., 2007. *Fundamentals of heat and mass transfer*. 6th ed., John Wiley & Sons, New York.

Kayansan, N., Karabacak, R., 1992. “Natural convection heat transfer coefficients for a horizontal cylinder with vertically attached circular fins”. *Heat Recovery Systems & CHP,* Vol 12, No 6, pp.457-468.

Kundu, P. K., Cohen, I. M., 2002. *Fluid Mechanics*. 2th ed., Academic Press, USA.

Menter, F. R., 1994. “Two-Equation Eddy Viscosity Turbulence Models for Engineering Applications”. AIAA Journal, Vol. 32, No. 8, pp. 1598-1605.

Menter, F. R., Kuntz, M., e Langtry, R., 2003. “Ten years of industrial experience with the SST turbulence model”. Turbulence, Heat and Mass Transfer 4, Begell House, Inc

Souza, S. I. S., Bessa, K. L., Maurente, A., 2019. “Numerical investigation of convection in tubes with aluminum and carbon steel fins: evaluating the assumption of convective heat transfer coefficient as that for the tube without fins and relating physical processes with the optimum spacing between fins”. Journal of the Brazilian Society of Mechanical Sciences and Engineering, Vol. 41, pp. 114

Yaghoubi, M., Mahdavi, M., 2013. “An investigation of natural convection heat transfer from a horizontal cooled finned tube”. *Experimental Heat Transfer,* Vol 26, pp.343-359.

Wilcox, D. C., 1994. Turbulence Modeling for CFD, DCW Industries, USA.

8. RESPONSIBILITY NOTICE

The authors are the only responsible for the printed material included in this paper.